

Effect of welding parameters on the strain rate and microstructure of friction stir spot welded 2024 aluminum alloy

Adrian Gerlich · Peter Su · Motomichi Yamamoto · Tom H. North

Received: 24 July 2006 / Accepted: 3 October 2006 / Published online: 4 April 2007
© Springer Science+Business Media, LLC 2007

Abstract The stir zone microstructure, crystallographic texture, temperature and strain rate in the stir zones produced during Al 2024 spot welding using different tool rotational speed settings are investigated. The calculated strain rate during spot welding decreases from 1600 to 0.6 s^{-1} when the tool rotational speed increases from 750 to 3000 rpm. The low strain rate values are associated with tool slippage resulting from spontaneous melting of S phase particles at temperatures $\geq 490 \text{ }^\circ\text{C}$. However, the calculated strain rate is 1600 s^{-1} in Al 2024 spot welds made using tool rotational speed of 750 rpm since the temperature never reaches $490 \text{ }^\circ\text{C}$. Material transfers downwards via that pin thread during the dwell period in Al 2024 spot welding. It is proposed that this downward transfer of material provides a continuous supply of undissolved S phase particles, which melt spontaneously when the welding parameter settings produce stir zone temperatures $\geq 490 \text{ }^\circ\text{C}$. A weak crystallographic texture where the $\{100\}$ planes are oriented at about 45° to the θ -direction exists in the stir zones of spot welds made using different tool rotational speeds (from 750 to 3000 rpm). Another crystallographic texture where the $\{100\}$ planes are parallel to the Z-direction (to the tool axis) is stronger in spot welds made using higher tool rotational speed settings. Also, material located at the root of the pin thread has a quite different crystallographic texture from that in the bulk of the stir zone.

Introduction

The friction stir welding process was developed by TWI, Abington, UK in 1991 for joining aluminum alloys [1]; subsequently the process has been used during joining of magnesium, titanium and copper alloys, stainless steel and thermoplastics in thicknesses ranging from 1 to 50 mm [2–7]. The detailed microstructural features and mechanical properties of friction stir seam welds in Al 2024 alloy sheet have been widely studied [8–16].

Friction stir spot welding is a process variant where the rotating tool is plunged into and out of two overlapping sheets at a particular location. A stir zone comprising dynamically recrystallized material is created in a cycle time, which is typically in the range from 2 to 5 s. A keyhole region remains in the welded component when the rotating tool is retracted, although it can be filled via the use of a specially-designed tool fixture [17]. Although the factors determining tool penetration and the mechanical properties have been investigated during friction stir spot welding of different aluminum and magnesium alloy sheet materials [18–21], the microstructural features of Al 2024 spot welded joints have not been investigated in detail.

Frigaard et al. [22] suggested strain rate values from 1.6 to 17 s^{-1} found during friction stir seam welding of Al 6082 and Al 7108 were associated with local melting of second-phase particles, which facilitated tool slippage at the contact interface between the periphery of the rotating tool and adjacent material in the stir zone. North et al. [23] also proposed that local melting and tool slippage could account for the low travel speeds that are obtainable during friction stir seam welding of Al 2024 and Al 7075 sheets. Local melting has been recently observed at grain boundary regions in Al 7010 friction stir seam welds made using a combination of high travel speed and tool rotational

A. Gerlich (✉) · P. Su · M. Yamamoto · T. H. North
Department of Materials Science & Engineering,
University of Toronto, 184 College St., Rm. 140, Toronto, ON,
Canada M5S 3E4
e-mail: gerlich@ecf.utoronto.ca

speed settings [24]. Also, Gerlich et al. [25] suggested that spontaneous melting of second-phase particles (η , S and T phases) accounted for the substantial decrease in calculated strain rate values (from 650 to about 20 s⁻¹) when the tool rotational speed increased from 1500 to 3000 rpm during Al 7075-6 friction stir spot welding. In direct contrast, strain rate values of around 1000 s⁻¹ have been reported during numerical modeling of the shear layer formed immediately adjacent to the rotating pin during Al 2024 friction stir seam welding [26].

In the present paper the strain rate in the stir zone region of Al 2024 friction stir spot welds is estimated using the Zener–Hollomon relation. EBSD and TEM microscopy are used to determine the average subgrain dimensions in the stir zones of Al 2024 spot welds made using different tool rotational speed settings. The temperature cycle during Al 2024 spot welding is determined by locating thermocouples within the welding tool itself, at the locations 200 μm from the tip of the rotating pin and midway between the pin and tool shoulder peripheries. The crystallographic textures in the stir zones of Al 2024 spot welds made using different welding parameter settings are investigated. The crystallographic textures in material retained at the root of the pin thread and in the bulk of the stir zone are also compared.

Experimental procedure

Table 1 shows the chemical composition of the 6.3 mm thick Al 2024 T351 sheet used during this investigation.

The tool employed during friction stir spot welding had a shoulder diameter of 10 mm, a pin diameter of 4 mm and a pin length of 2.2 mm. The tool was made of H13 steel (0.35 wt.% C, 5 wt.% Cr, 1.5 wt.% Mo, 1 wt.% V) steel and had a hardness of 46–48 HRC and a simple threaded pin profile. The plunge rate during all spot welding trials was 2.5 mm/s while the specified tool penetration depth was 2.2 mm. This penetration depth corresponded with the point when the tool shoulder just contacted the upper surface of the sheet. The welding cycle was extended by incorporating a dwell time of up to 4 s once the rotating pin was fully penetrated. The tool rotational speed remained constant while axial force and torque decreased during the 4 s long dwell period and due to machine compliance the rotating tool penetrated up to 200 μm into the surface of the sheet.

The influence of tool rotational speed variations from 750 to 3000 rpm on the average subgrain dimensions and

temperature in the stir zone was investigated. The stir zones from spot welds in a monolithic 6.3 mm plate as well as overlapping 1.5 mm sheets were studied. Since almost all of the energy generated during friction stir spot welding is due to the torque resulting from tool rotation [21], stir zones made using rotational speeds ≤ 750 rpm did not have bonded regions having acceptable dimensions and joint mechanical properties [27, 28]. In the present investigation the welding parameters used are those that produced stir zones having widths >100 μm .

The thermal cycle during friction stir spot welding was measured by embedding 0.25 mm diameter K-type thermocouples at the location 0.20 mm from the tip of the rotating pin and 0.8 mm from the outer periphery of the tool shoulder. During all temperature measurements the thermocouple junction was always in direct contact with dynamically recrystallized material formed during the spot welding operation. A detailed description of the temperature measurement set-up has been provided elsewhere [25]. All temperature measurements were repeated at least three times at each welding parameter setting. The variation in temperature during the 4 s dwell period was <7.4 °C during repeat testing. The error bars shown on any figure indicate one standard deviation above and below the reported value.

The temperature cycle in Al 2024 material beneath the tool shoulder was measured since this provided information concerning that thermal cycle in that location and the cooling rate following completion of the spot welding operation. Both air-cooled and rapidly-quenched spot welded joints were examined. The spot welds were rapidly-quenched in a mixture of methanol and liquid nitrogen at a temperature of -80 °C immediately following tool retraction. Prior to spot welding 0.25 mm diameter K-type thermocouples were located 0.7 mm below the upper surface of the Al 2024 sheet at a distance of 1.3 mm from the periphery of the rotating pin. Following spot welding the locations of the thermocouples were determined using transverse sectioning and metallographic examination. All test sections were etched using Keller's reagent.

Transmission electron microscopy (TEM) was performed using a Hitachi H-800 machine operating at 200 kV. All test samples were thinned using a twin-jet electropolishing technique in a solution of 25 vol.% of HNO₃ and 75 vol.% of methanol at a temperature of -30 °C and a voltage of 12 V. The average grain dimensions in the stir zone were determined using planimetry by examining at least 50 grains on each TEM specimen.

Table 1 Chemical composition, wt%

Element:	Cu	Mg	Mn	Fe	Zn	Si	Ti	Cr	Al
Al 2024-T351	4.30	1.42	0.62	0.15	0.07	0.07	0.03	<0.01	bal.

Electron backscattered diffraction (EBSD) was also used to obtain detailed quantitative information concerning the stir zone microstructure. The surface of each sample was ground using 1200 grit SiC prior to EBSD examination and final electro-polishing was carried out using identical preparation conditions to those during TEM microscopy. The step size was 0.25 μm to 0.3 μm during EBSD while the angular resolution limit of the equipment was about 2° . The grain boundary statistics and crystallographic textures were determined using a Hitachi S-4500 field emission scanning electron microscope with TSL TexSEM software. Figure 1 shows a schematic of a spot welded cross-section. Region I, located 100 μm from the keyhole periphery halfway up the rotating pin, was examined using TEM and EBSD. During EBSD all misorientation output was processed using a ‘clean-up’ algorithm where individual points not belonging to a neighboring grain and points indexed with less than 1% confidence were interpolated to the average orientation of neighboring points. The average EBSD grain dimensions were calculated from misorientation maps using the linear intercept method; only grain boundaries having $>2^\circ$ misorientations were considered. It has already been shown that the average subgrain dimensions found using TEM are similar to those estimated using EBSD when the 2° misorientation criterion is applied during the examination of the stir zones produced in Al 7075 and Al 5754 friction stir spot welds [25, 29].

Pole figures were used to evaluate the crystallographic textures in the stir zones of spot welds produced using different tool rotational speed settings. The Z-direction and (θ) orientation directions are shown in Fig. 1. The crystallographic texture of material retained at the root of the pin thread was also compared to that in the bulk of the stir zone.

As mentioned earlier, Gerlich et al. [25] recently associated tool slippage with spontaneous melting of second-phase particles (η , S and T phase) during the dwell period in Al 7075-T6 spot welding. During the dwell period in spot welding the incorporated material is transferred downwards via the pin thread and into the stir zone [30].

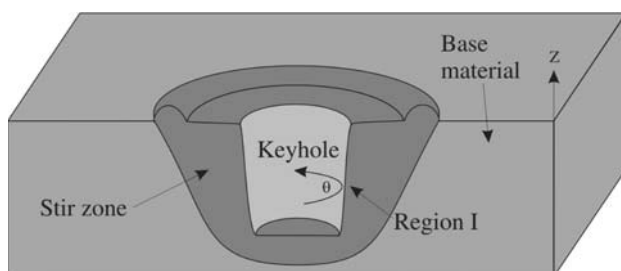


Fig. 1 Schematic of a friction stir spot weld showing Region I, which was examined using both TEM and EBSD microscopy

The downward transfer of material via the pin thread was investigated during the dwell period in Al 2024 spot welding was examined in spot welds made between 1.5 mm thick cold-rolled and 6.3 mm thick sheets. The 1.5 mm thick sheet was solution-treated at 470 $^\circ\text{C}$ and then cold rolled, with the process being carried out in 3 steps to achieve a reduction in thickness of 80%. A combination of optical microscopy and crystallographic texture analysis were used when comparing material located in the root of the pin thread with that in bulk of the stir zone.

The downward movement of Al_2O_3 tracer particles via the pin thread during the dwell period in Al 2024 spot welding was investigated in the following manner. The rotating pin was fully penetrated into the 6.3 mm thick Al 2024 sheet and was then withdrawn at the end of a 1 s dwell period. Eight 0.4 mm diameter \times 1 mm deep holes were then drilled around the circumference of the keyhole at the radial location 1 mm from the keyhole periphery. The drilled holes were then filled with Al_2O_3 powder. The spot welding operation was then repeated using identical welding parameter settings with the addition of a 2 s long dwell period. Tool rotation was suddenly terminated during the spot welding operation. The movement of tracer particles was investigated by sectioning both the steel tool and the stir zone formed during Al 2024 spot welding.

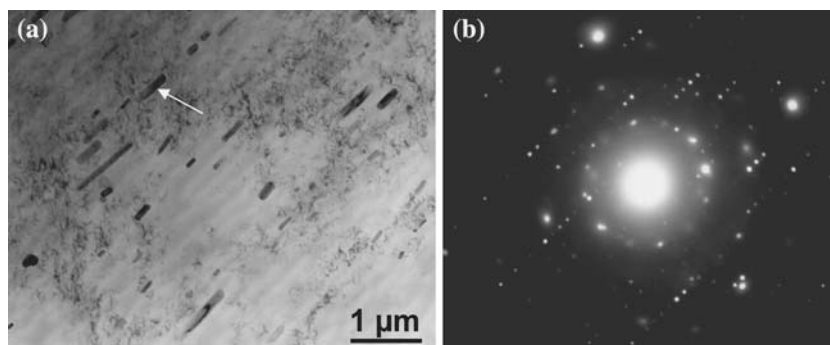
Results

The as-received Al 2024 sheet comprised elongated grains having average dimensions of 130 μm parallel to the rolling direction and 50 μm in the through-thickness direction. The majority of the second-phase particles in the as-received sheet comprised Al_2Cu and S phase (Al_2CuMg). These precipitates are typically found in this particular Al-alloy [31]. Figure 2a shows the typical morphologies of incoherent particles in the α -Al matrix while Fig. 2b shows the selected area diffraction pattern (SADP) from an incoherent particle, which has an orthorhombic structure and closely corresponds with S phase. The 100 nm wide by 0.5 μm long S phase particle has a rod-like shape.

Figure 3 shows the pin temperature and torque output during Al 2024 spot welding using a tool rotational speed of 3000 rpm. The dwell period extends from 1.25 to 5.25 s in this particular figure. The temperature at the location 200 μm from the tip of the rotating pin increases to 501 $^\circ\text{C}$ during the 4 s dwell period in spot welding. The highest temperature measured during Al 2024 spot welding using a tool rotational speed of 3000 rpm was 504 $^\circ\text{C}$.

The average temperature and the heating rate during spot welding increased when higher tool rotation speed settings were employed, see Fig. 4a, b. The average

Fig. 2 (a) TEM micrograph of base material containing Al_2CuMg particle (see arrow). (b) SAD pattern from the Al_2CuMg particle



heating rate of the pin during the tool penetration stage in spot welding (in the period from 0.3 to 1.3 s) increased from 212 to 385 °C/s when the tool rotational speed increased from 750 to 3000 rpm. The average pin temperature increased from 410 to 497 °C when the rotational speed increased in a similar manner. Although the shoulder experienced much higher heating rates during spot welding lower average temperature values were measured by the thermocouple, which was embedded in the tool shoulder. Lower tool shoulder temperatures were measured since

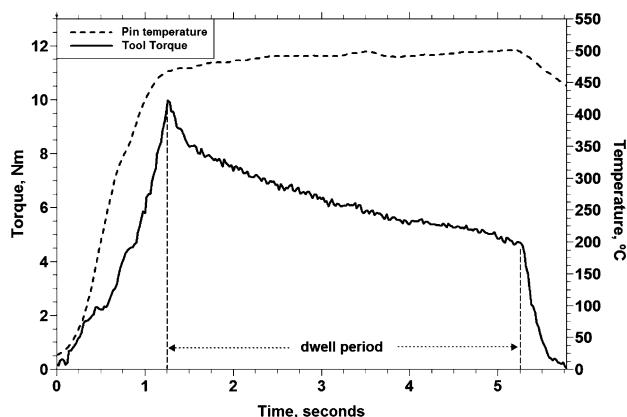
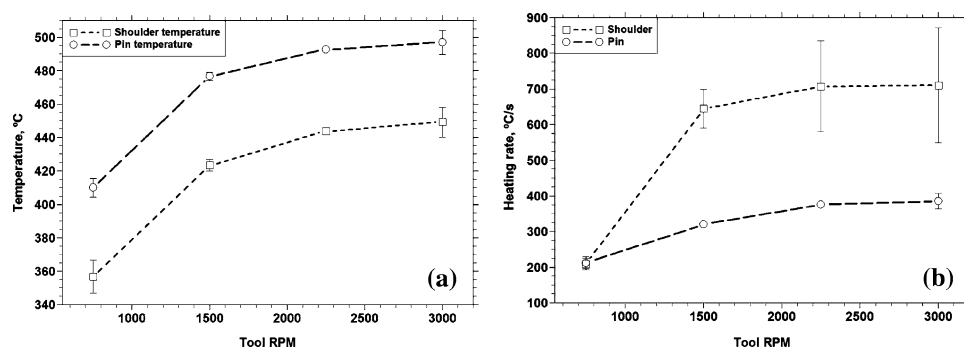


Fig. 3 Tool torque and pin temperature output during friction stir spot welding of Al 2024 using a tool rotational speed of 3000 rpm. The dwell period extends from 1.25 to 5.25 s

Fig. 4 (a) The relation between tool rotational speed and the average temperature during spot welding using a dwell time of 4 s. (b) The heating rate during spot welding when different tool rotational speeds are applied. The error bars indicate standard deviations of temperature at any rotational speed setting



spot welding was terminated when the rotating pin was fully penetrated and the tool shoulder just contacted the upper sheet surface.

Figure 5 shows the temperature cycle in the location 0.7 mm below the base of the tool shoulder and at a distance of 1.3 mm from the keyhole periphery. The average temperature was much less than that measured using the thermocouple, which was embedded within the tool itself, e.g. 412 and 497 °C. It is well-documented that temperature decreases markedly at small distances from a contact surface, which is frictionally heated [32, 33]. The temperature decreased from 410 °C to 200 °C in around 4.6 s in air-cooled spot welds. In rapidly quenched spot welds the temperature decreased from 390 °C to 200 °C in about 2.3 s, see Fig. 5.

Figure 6 shows EBSD misorientation maps for the stir zone regions in welds produced using different rotational speed settings (from 750 to 3000 rpm). The average sub-grain size increased from 0.57 μm in spot welds made using a rotational speed of 750 rpm to 1.23 μm in spot welds produced using a rotational speed of 3000 rpm, see Table 2. However, the fraction of high angle boundaries was almost constant at about 97% in the spot welds made using different rotation speeds.

Figure 7 shows TEM micrographs of the stir zone produced in spot welds made using different tool rotational speed settings. It is apparent from Table 2 that the average

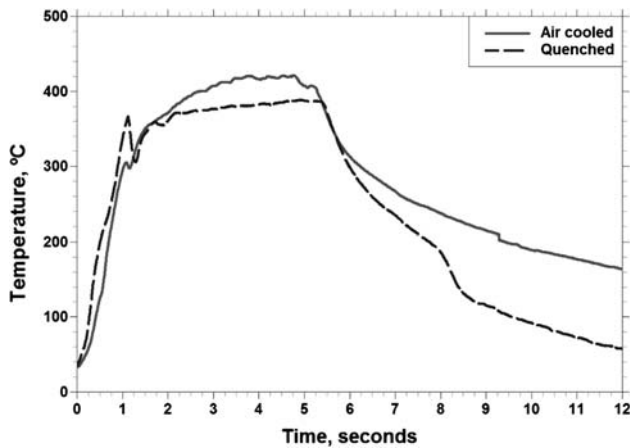
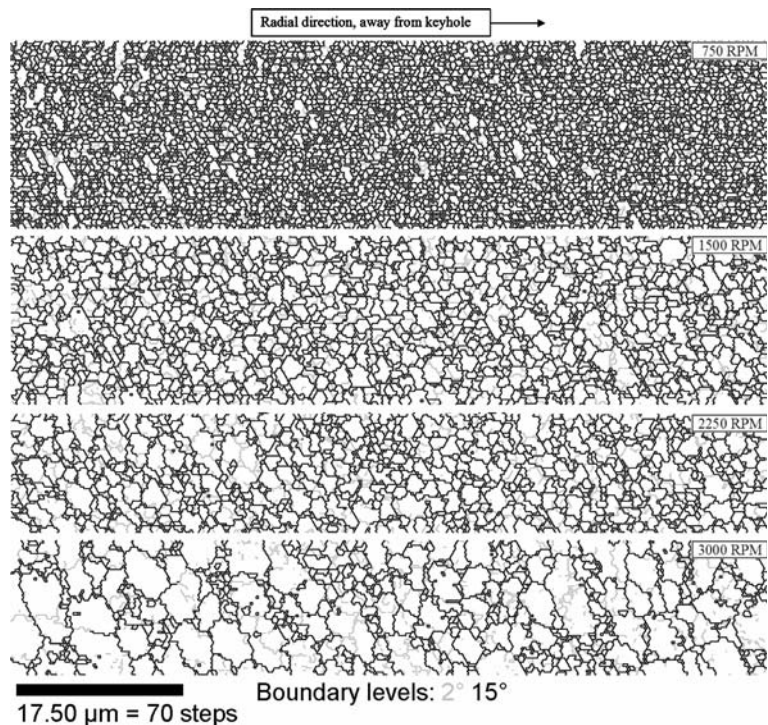


Fig. 5 Temperature cycle at the location 0.7 mm below the tool shoulder in an Al 2024 spot weld produced using a tool rotational speed of 3000 rpm, and a dwell time of 4 s

subgrain dimensions estimated using TEM microscopy corresponded well with the values determined using EBSD.

Figure 8 shows the crystallographic textures in the stir zones of joints made using different tool rotational speeds. The {111} and {100} pole figures indicate that two textures are present. The {100} planes are oriented about 45° to the θ -direction while the {110} planes are orthogonal to both the Z- and θ -directions. Another texture component where the {100} planes are parallel to the Z-direction is much stronger in spot welds made using a tool rotational speed of 3000 rpm.

Fig. 6 EBSD misorientation maps showing subgrain boundaries with 2–15° misorientation (gray lines) and grain boundaries with >15° misorientation (black lines). From the stir zones of spot welds produced using tool rotational speeds of 750–3000 rpm and a dwell time of 4 s



The strain rate can be determined by incorporating the average subgrain size and the average temperature values in the stir zone in the Zener–Hollomon relation:

$$Z = \dot{\epsilon} \exp\left(\frac{Q}{RT}\right), \tag{1}$$

where Z is the Zener–Hollomon parameter (the temperature compensated strain rate), $\dot{\epsilon}$ is the strain rate, T is the deformation temperature, Q is the activation energy and R is the universal gas constant [34]. For a number of aluminum alloys the Zener–Hollomon parameter and the subgrain diameter, d , are related as follows [35–40]:

$$d^{-1} = a + b \log(Z), \tag{2}$$

where a and b are constitutive constants. Equations 1 and 2 were used to estimate the strain rate in the stir zone of spot welds produced using different rotational speed settings. The constitutive constants used during all calculations were those reported by Sheppard [41] when examining Al 2014 material, namely $Q = 144$ kJ/mol, $a = -1.095$ and $b = 0.087$. The calculated strain rate decreased from 1600 to 0.6 s⁻¹ when the tool rotation speed increased from 750 to 3000 rpm, see Fig. 9.

A number of Al 2024 spot welds made using rotational speeds of 750 and 3000 rpm were rapidly quenched immediately in a mixture of methanol and liquid nitrogen at a temperature of -80 °C following tool extraction. Void

Table 2 Average subgrain dimensions and grain boundary misorientation statistics determined using EBSD and TEM

RPM	EBSD Average subgrain dimensions (μm)	EBSD 2° to 15° Boundaries	EBSD >15° Boundaries	TEM Average subgrain dimensions (μm)
750	0.57 \pm 0.02	1.6%	98.4%	0.62 \pm 0.09
1500	0.80 \pm 0.06	2.2%	97.8%	–
2250	0.87 \pm 0.09	2.8%	97.2%	–
3000	1.23 \pm 0.21	3.1%	96.9%	1.57 \pm 0.44

formation was observed at inter-granular regions in TEM foils extracted from the stir zones of rapidly quenched Al 2024 spot welds produced using a rotational speed of 3000 rpm, see Fig. 10. The voids were found in locations several microns far from the thinnest edge of the TEM foil. However, voids were not observed in the TEM foils extracted from the stir zones of rapidly quenched spot welds made using a tool rotational speed of 750 rpm.

Discussion

Stir zone temperature

The average temperature during the dwell period in Al 2024 spot welding increases when higher tool rotational

speeds are applied, see Fig. 4a. Yang et al. [42] also reported that the average temperature increased from about 320 °C to above 500 °C when the tool rotational speed increased from 215 to 360 rpm during Al 2024 friction stir seam welding. It is worth noting that although much higher tool rotational speeds are used during spot welding the power inputs during seam and spot welding operations are similar (from 2 to 3 kW). The large difference between the temperature values found in Al 2024 friction stir seam and spot welds can be explained in the following manner. It is well-documented that the temperature markedly decreases at small distances from the contact interface [32, 33] and therefore the precise location of the thermocouple with respect to the rotating tool and shoulder periphery becomes a critical issue [30]. The results shown in Figs. 4a and 5 show that the average temperatures measured by the ther-

Fig. 7 TEM micrographs of the stir zone in spot welds made using tool rotational speeds of (a) 750 rpm and (b) 3000 rpm

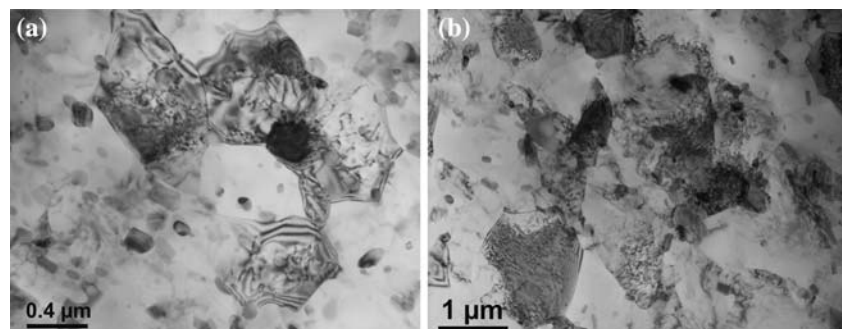
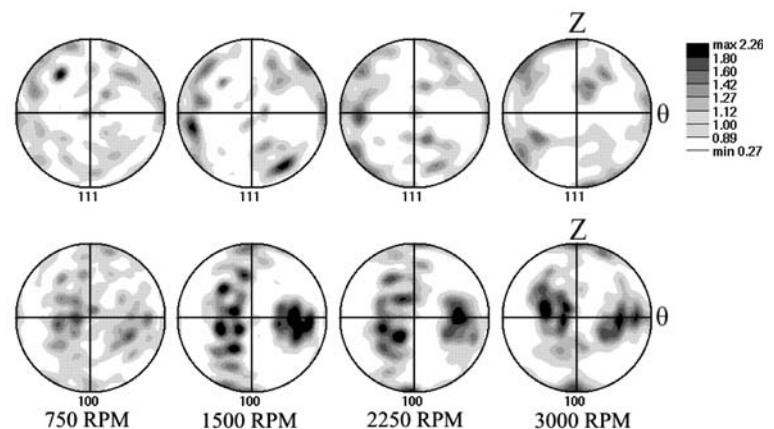


Fig. 8 {111} and {100} pole figures for the stir zones of spot welds made using tool rotational speeds from 750 to 3000 rpm



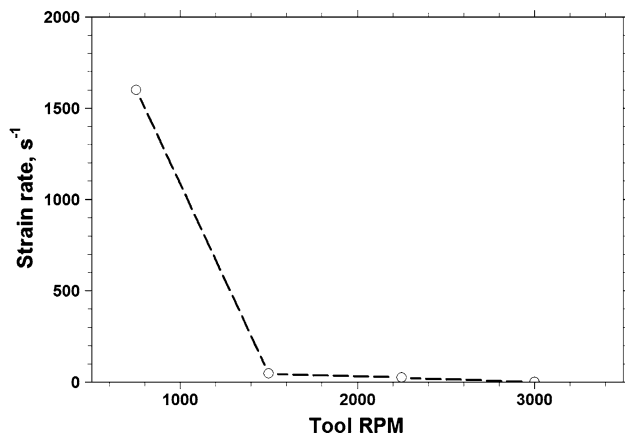


Fig. 9 Relation between the calculated strain rate and the tool rotational speed in Al 2024 spot welds

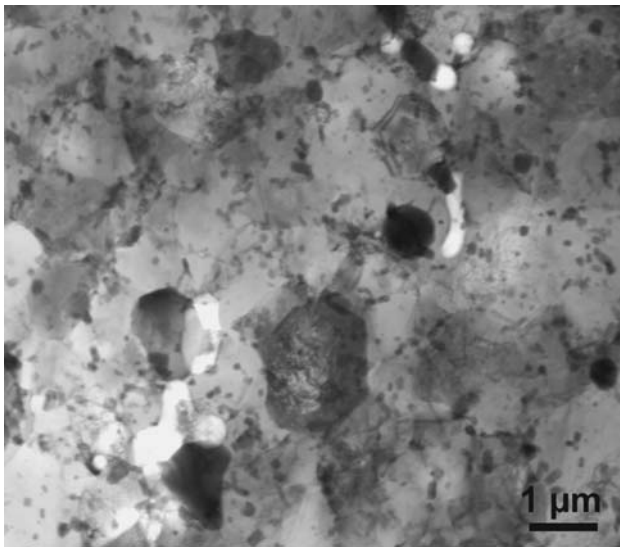


Fig. 10 TEM micrograph showing voids. In stir zone of an Al 2024 spot weld made using a tool rotation speed, and a dwell time of 4 s

mocouples located within the tool itself and in the location 0.7 mm from the base of the tool shoulder are markedly different, e.g. 412 and 497 °C. Temperature measurement during friction stir seam welding generally involves locating thermocouples at specific locations ahead of the traversing tool. However, it is also particularly difficult to obtain consistent temperature output when temperature is measured in this manner. The precise locations of thermocouples relative to the periphery of the rotating pin and the base of the tool shoulder will vary from one test to another. Also, it has been shown that dynamically recrystallized material produced during stir zone formation can displace thermocouples from their original locations [30].

The average temperatures at the location 200 μm from the tip of the rotating pin approach the solidus temperature of Al 2024 (502 °C [43]) during the dwell period in spot

welding, see Fig. 4a. Lower average temperatures are produced in joints made using lower rotational speed settings since the heating rate early in spot welding operation (in the period from 0.3 to 1.3 s) decreases from 385 to 212 °C/s, see Fig. 4b. The heating rate early in spot welding has a major influence on the average temperature in spot welds when the dwell time is set at 4 s. The solidus temperature is approached in Al 2024 spot welds made using rotational speed from 1500 to 3000 rpm when the dwell time is extended to 10 s [30].

Stir zone grain size and crystallographic texture

Similar average subgrain dimensions were found using TEM and EBSD microscopy when a 2° misorientation criterion was applied, see Table 2. TEM and EBSD microscopy also produced comparable grain size estimates in the stir zones of Al 7075 and Al 5754 spot welds [25, 29]. The average subgrain dimensions in Al 2024 spot welds ranged from 0.57 to 1.23 μm, see Table 2. It is unlikely that the fine-grain microstructures found in Al 2024 stir zones are associated with particle stimulated nucleation since the formation and growth of nuclei are limited when the Zener–Hollomon parameter is in the range from 10^9 to 10^{14} s⁻¹ [50]. Average grain sizes ranging from 1 to 6.4 μm have been reported in Al 2024 friction stir seam welds [44–49]. However, average grain sizes <1 μm are only produced when friction stir seam welds are rapidly cooled [44].

The crystallographic textures in the stir zones of Al 2024 spot welds are quite different from those found during torsion testing of aluminum and copper alloys [51]. A weak {001}<110> texture component is indicated in Fig. 8. It is well-known that torsional textures are not preserved when high total strains are applied [52] and values of 40–80 have been reported during friction stir welding [53]. Also, since grain boundary sliding is important during stir zone formation [30, 54, 55] this will favor texture randomization [56].

The pole figures found when examining Al 2024 spot welds are quite different from those reported in the stir zones of friction stir seam welds. Strong <111> textures parallel to the tool axis have been reported in friction stir seam welds [46, 57]. The texture components found in friction stir seam welds may be associated with grain growth when the joints cool to room temperature [50, 58]. However, no evidence of grain growth following friction stir spot welding has been reported [25, 29].

Estimating the strain rate

Although Eqs. 1 and 2 provide a ready means of estimating the strain rate during the friction stir spot welding operation

the validity of the calculated strain rate values depend remarkably on the precision with which temperature and grain size are measured. Satisfactory strain rate estimates can be determined provided that:

- a) There is limited scatter in the average temperatures and average subgrain dimensions when they are measured in similar locations relative to the periphery of the rotating tool. Small changes in the average grain dimensions and average peak temperature values produce large changes in estimated strain rate values [25]. Fortunately, the temperature cycle within 200 μm of the bottom of the rotating pin can be measured both reliably and with little scatter in measured values during friction stir spot welding, see Fig. 4a. Also the average subgrain dimensions at the location 100 μm from the keyhole periphery can be readily determined using TEM and EBSD, see Table 2.
- b) There is negligible grain growth when the joint cools to room temperature. Gerlich et al. [25, 29] have already confirmed that there is no evidence of grain growth when Al 7075-T6 and Al 5754 alloy friction stir spot welds cool to room temperature. Similar output was found during Al 2024 spot welding. For example, the average subgrain size is 1.23 μm in the stir zones of air-cooled Al 2024 spot welds made using a tool rotational speed of 3000 rpm. In rapidly-cooled spot welds made using identical welding parameter settings the average subgrain size is 1.35 μm . In direct contrast, it has been reported that significant grain growth occurs when friction stir seam welds cool to room temperature [58].

The calculated strain rate during Al 2024 spot welding decreases from 1600 to 0.6 s^{-1} when the tool rotational speed increases from 750 rpm to 3000 rpm, see Fig. 9. The expected shear rate is around 525 s^{-1} when a non-slip condition is assumed at the contact interface between the periphery of the rotating tool and adjacent material in the stir zone in spot welds made using a rotational speed of 3000 rpm. Also, as pointed out earlier, strain rate values of around 1000 s^{-1} were reported during numerical modeling of the shear layer, which forms immediately adjacent to the rotating pin in Al 2024 friction stir seam welds [26].

Gerlich et al. [25] also found a similar relation between tool rotational speed and calculated strain rate values during Al 7075-T6 friction stir spot welding. The steep decline in calculated strain rate values in Al 7075-T6 spot welds produced using high tool rotational speed settings was attributed to spontaneous melting of undissolved second-phase particles (η , β S and T phases) at temperatures ≥ 475 $^{\circ}\text{C}$. Similarly, Frigaard et al. [22] reported strain rate values from 1.6 to 17 s^{-1} during friction stir seam welding of Al 6082 and Al 7108 and suggested that local melting of

second-phase particles facilitated tool slippage at the contact interface. Frigaard's local melting proposal was based on the results of prior research carried out by Dronen et al. [59] who confirmed that spontaneous melting of second phase particles such as η and T phase occurred when Al–Zn–Mg test sections were upquenched at about 35 $^{\circ}\text{C}/\text{s}$. Similar results were found by Reiso et al. [60] during rapid upquenching of Al–Cu alloy test sections. It is apparent from Fig. 4b that the heating rates during Al 2024 spot welding are much higher than those employed during upquenching investigations.

Large numbers of S phase (Al_2CuMg) particles are present in the as-received Al 2024 sheet, see Fig. 2. Since S phase melts spontaneously at 490 $^{\circ}\text{C}$ [61] and high heating rates occur during Al 2024 spot welding, there is a strong likelihood that undissolved S phase particles will melt spontaneously at when the stir zone temperature equals or exceeds 490 $^{\circ}\text{C}$. Fig. 4a shows that the average temperature 200 μm from the tip of the rotating pin exceeds 490 $^{\circ}\text{C}$ in spot welds made using rotational speeds of 2500 and 3000 rpm. Also, an average temperature of 477 ± 3 $^{\circ}\text{C}$ is attained in spot welds made using a rotational speed of 1500 rpm. However, the temperature never reaches 490 $^{\circ}\text{C}$ in spot welds made using a tool rotational speed of 750 rpm and the calculated strain rate is 1600 s^{-1} , see Figs. 4a and 9. It is therefore proposed that the low calculated strain rate values found in Al 2024 spot welds produced using rotational speeds from 1500 to 3000 rpm result from spontaneous melting of S phase particles and tool slippage at the contact interface between the tool periphery and adjacent material in the stir zone.

A number of investigators have provided metallographic evidence of local melting during both friction stir seam welding and in friction stir spot welding operations. For example, evidence of local melted film formation has been found in Al 2024-T3 friction stir welds [62], in Al 6061-T6/ Al_2O_3 MMC plunge tests [63], in dissimilar Al 6111/AZ91 spot welds [64] and in dissimilar 1050/AZ31 friction stir welds [65]. Although it is possible that the voids in Fig. 10 may be indicative of local melting when eutectic material located at grain boundary regions is preferentially attacked during the electro-polishing stage in TEM foil preparation, they might simply be artifacts resulting from TEM specimen preparation. Voids were not detected in spot welds made using a tool rotational speed of 750 rpm. It is possible that they may have been present in spot welds produced using all welding parameter settings due to the limited number and small dimensions of TEM samples, which were examined. In this connection, voids have also been observed on the fracture surfaces of broken tensile samples which were machined from dissimilar Al 2024/Al 7075 friction stir welds [66]. However, since the tensile test specimens fail as a result of ductile fracture this makes it

particularly difficult to confirm whether the voids observed in dissimilar Al 2024/Al 7075 friction stir welds bear any relation to those shown in Fig. 10.

The likelihood of finding metallographic evidence confirming local melting in the stir zones produced during Al 2024 spot welding will depend on the kinetics of dissolution of liquid droplets at 490 °C, the factors determining the supply of undissolved S phase particles during the dwell period and particle dissolution when spot welds cool to room temperature.

Local melting and dissolution during the dwell period

The dissolution kinetics of spontaneously melted droplets has been investigated by Rieso et al. [60]. Using Whelan’s methodology [67], the approximate time required for dissolution of a spherical liquid droplet is determined by the relation:

$$\left(\frac{R}{R_o}\right)^2 = 1 - \frac{kD}{R_o^2}t \tag{3}$$

where R is the radius of the spherical droplet, R_o is the initial radius, D is the diffusion rate and t is time in seconds. k is the driving force for solute diffusion and can be calculated as follows:

$$k = 2 \left[\frac{C_{T_2}^{\alpha/liq} - C_{T_1}^{\alpha/\beta}}{C_{T_2}^{liq/\alpha} - C_{T_2}^{\alpha/liq}} \right] \tag{4}$$

$C_{T_1}^{\alpha/\beta} = 5.7$ wt.%, $C_{T_2}^{\alpha/liq} = 5.9$ wt.% and $C_{T_2}^{liq/\alpha} = 39.4$ wt% and are derived from the Al–Al₂CuMg quasi-binary section in the Al–Mg–Cu ternary phase diagram [68]. The driving force for solute diffusion and dissolution is $k = 0.0119$, see the Appendix.

Figure 11 shows the relation between time available for dissolution and the radius of spherical liquid droplets. During all calculations it is assumed that droplet dissolution is determined by Mg diffusion in aluminum and that D_{Mg} in Al = 0.24 μm²/s at 490 °C [69]. Tundal et al. [70] have already confirmed that the diffusion rate of the element, which has the lowest chemical concentration in the alloy, provides the best approximation in a ternary treatment of diffusion problems.

A 200 nm diameter spherical liquid droplet formed at the start of the dwell period will be completely dissolved in 4 s, see Fig. 11. The dissolution of spherical liquid droplets is assumed since it has already been shown that elongated, rod-like intermetallic particles are broken up during friction stir seam welding [71] and alumina particles are fragmented within the pin thread during friction stir spot welding [72]. However, the time available for dissolution

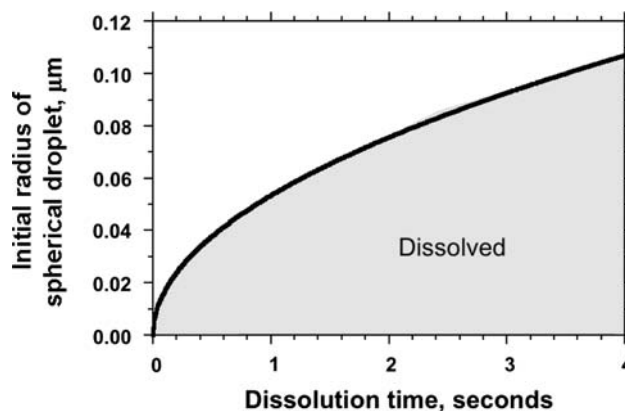


Fig. 11 Relation between the initial radius of a spherical liquid droplet and the time available for dissolution during the dwell period in Al 2024 spot welding

of a liquid droplet will depend on when the spontaneous melting event occurs during the dwell period in Al 2024 spot welding. It has been shown recently that the dimensions of the stir zone immediately adjacent to the periphery of the rotating pin are markedly increased since material from the locations beneath the tool shoulder and the bottom of the rotating pin is incorporated during the dwell period in spot welding [28, 30, 73]. As a result, material containing undissolved S phase particles will be introduced into the stir zone during the whole of the dwell period in spot welding.

The incorporation of material during the dwell period was investigated in spot welds between 1.5 mm thick cold-rolled and 6.3 mm thick Al 2024 sheets. Figures 12 and 13 show the microstructure and crystallographic texture of material located at the root of pin thread in an Al 2024 spot weld made using different dwell times. Material at the root of the pin thread and in the bulk of the stir zone has an

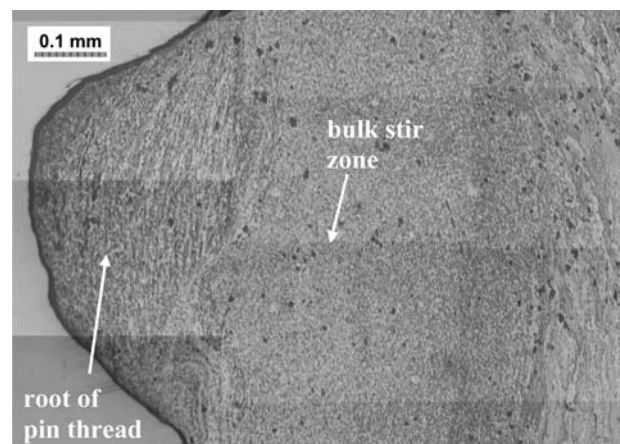
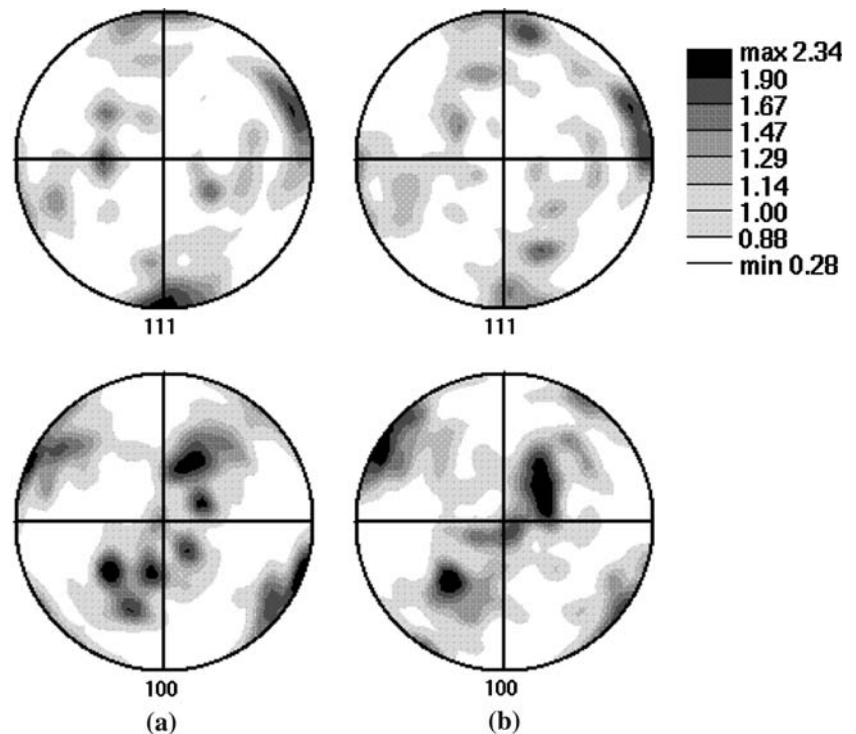


Fig. 12 Optical micrograph of material retained at the root of the pin thread. In an Al 2024 spot weld made using a dwell time of 1 s, and a tool rotational speed of 3000 rpm

Fig. 13 Pole figures for material retained at the root of the pin thread in Al 2024 spot welds produced using (a) a dwell time of 1 s and (b) a dwell time of 3 s

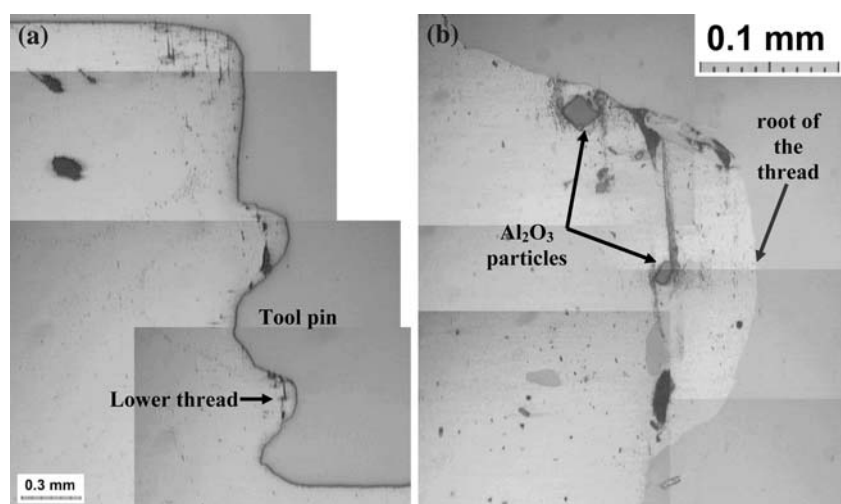


equiaxed microstructure with a grain size of about 1 μm . However, the crystallographic textures are quite different, e.g. the $\{111\}$ planes are parallel to the tool axis in material located at the root of the pin thread while the $\{100\}$ planes are parallel to the tool axis in the bulk of the stir zone (see Fig. 8). Although the results in Figs. 8 and 13 provide some measure of support for the contention that material is transferred downwards via the pin thread during the dwell period, it might be argued that the root of the pin thread is filled with material during the tool penetration stage in spot welding and is retained in this location during the whole of the dwell period in Al 2024 spot welding. For this reason, the downward movement of Al_2O_3 tracer material during the dwell period in spot welding was further investigated.

Figure 14 shows cuboidal Al_2O_3 tracer particles located at the root of the pin thread. These tracer particles originated from the location beneath the tool shoulder and were moved downwards via the pin thread during the 2 s long dwell period in spot welding.

Since material containing undissolved S phase is incorporated into the stir zone during the dwell period in spot welding the time available for dissolution of a liquid droplet will depend on when the local melting event occurs. For example, the time available for droplet dissolution will be 1 s when the spontaneous melting event occurs 3 s after the initiation of the dwell period. A 100 nm diameter liquid droplet will dissolve during this time interval.

Fig. 14 (a) Alumina tracer particles located at the root of the pin thread in an Al 2024 spot weld made using a tool rotational speed of 3000 rpm. (b) Detail of the lower thread showing cuboidal Al_2O_3 particles, which were moved downwards during the 2 s dwell period in spot welding



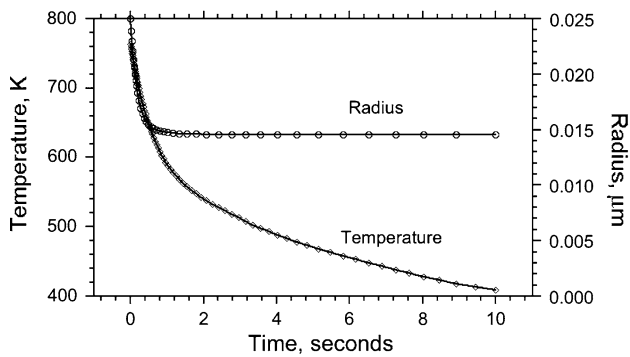


Fig. 15 Dissolution of a 50 nm diameter spherical particle when the Al 2024 spot weld cools to room temperature

When liquid droplets are not completely dissolved at the end of the dwell period the solidified particles will continue to dissolve as the spot weld cool to room temperature. Figure 15 shows the dissolution characteristics of a 50 nm spherical particle when the Al 2024 spot weld cool to room temperature. A detailed description of the calculation method is provided in the Appendix. The particle diameter will decrease from 50 nm to 30 nm during cooling. It is apparent from Figs. 11 and 15 that 100 nm diameter liquid droplets produced during spontaneous melting of S phase will dissolve unless they are formed close to the end of the dwell period in Al 2024 spot welding.

Conclusions

The stir zone microstructure, crystallographic texture, temperature and strain rate in the stir zones produced during Al 2024 spot welding using different tool rotational speed settings were investigated. The stir zone microstructure was examined using a combination of EBSD and TEM microscopy while the strain rate during spot welding was calculated by incorporating measured temperatures and the average subgrain dimensions in the Zener–Hollomon equation. It is concluded that:

1. The calculated strain rate during spot welding decreases from 1600 to 0.6 s⁻¹ when the tool rotational speed increases from 750 to 3000 rpm. The low strain rate values were associated with tool slippage resulting from spontaneous melting of S phase particles at temperatures ≥ 490 °C. In contrast, when a low tool rotational speed is used during spot welding (750 rpm) the temperature never reaches 490 °C and the calculated strain rate is 1600 s⁻¹.
2. Material transfers downwards via that pin thread during the dwell period in Al 2024 spot welding. It is suggested that this downward transfer of material provides a continuous supply of undissolved S phase particles, which

melt spontaneously when the welding parameter settings produce stir zone temperatures ≥490 °C.

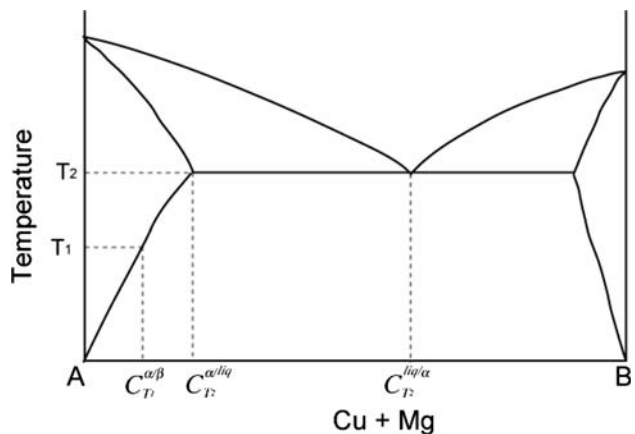
3. weak crystallographic texture where the {100} planes were oriented at about 45° to the θ-direction was found in the stir zones of spot welds made using different tool rotational speeds (from 750 to 3000 rpm). Another crystallographic texture where the {100} planes were parallel to the Z-direction (to the tool axis) was stronger in spot welds produced using higher tool rotational speed settings. In addition, material located at the root of the pin thread has a quite different crystallographic texture from that in the bulk of the stir zone.

Acknowledgements The authors wish to acknowledge financial support from the Natural Sciences and Engineering Research Council of Canada during this project.

Appendix

Dissolution of liquid droplets

The Al–Al₂CuMg quasi-binary section in the Al–Mg–Cu ternary phase diagram is shown below:



The driving force for diffusion and dissolution of Al₂CuMg is determined by the relation:

$$k = 2 \left[\frac{C_{T_2}^{\alpha/liq} - C_{T_1}^{\alpha/\beta}}{C_{T_2}^{liq/\alpha} - C_{T_2}^{\alpha/liq}} \right] = 2 \left[\frac{5.9 - 5.7}{39.4 - 5.9} \right] = 0.0119$$

where, $C_{T_1}^{\alpha/\beta} = 5.7\%$, $C_{T_2}^{\alpha/liq} = 5.9\%$, $C_{T_2}^{liq/\alpha} = 39.4\%$, at $T_2 = 508\text{ °C}$ [68]. The dissolution of Al₂CuMg is calculated at 490 °C since this temperature was attained in spot welds using >1500 rpm and is the reported melting temperature of this phase [61]. The diffusion coefficient of Mg in Al depends on the relation [69]:

$$D = D_o \exp \left[-\frac{Q}{RT} \right]$$

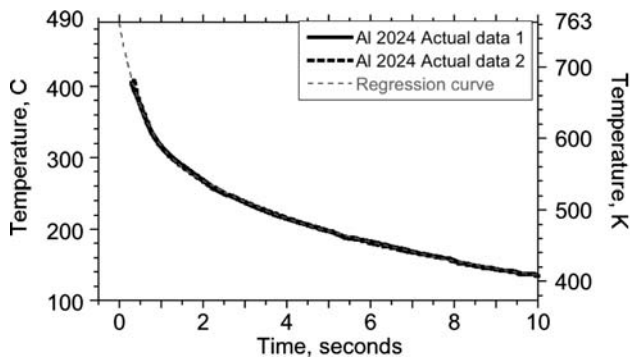
where, $D_o = 2.1 \times 10^7 \mu\text{m}^2/\text{s}$, $Q = 116 \text{ kJ/mol}$, $R = 8.314 \text{ J/mol K}$, $T = 763^\circ\text{K}$ (490°C), and thus $D_{\text{Mg in Al}} = 0.24 \mu\text{m}^2/\text{s}$.

The relation between the initial radius of the liquid droplet R_o and the time t available for dissolution at 490°C is determined by the relation:

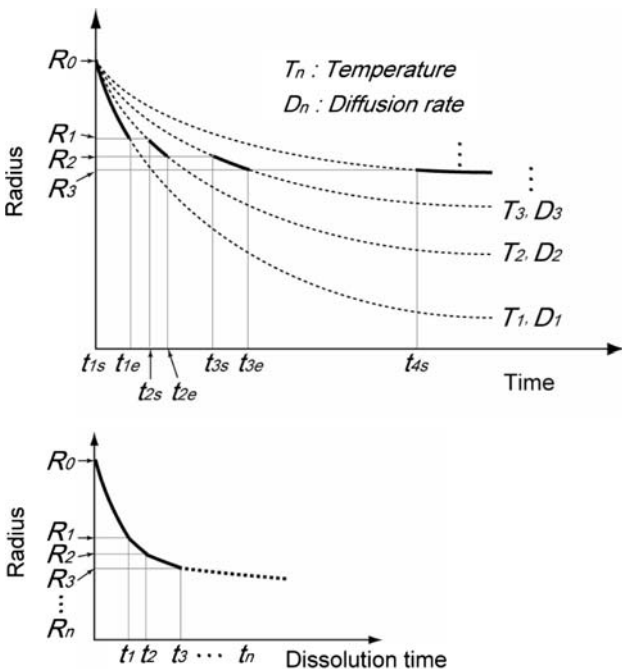
$$R_o = \sqrt{kD_{\text{Mg in Al}} \cdot t}$$

Dissolution when the Spot Weld Cools to Room Temperature

Figure 5 shows the thermal cycle when the Al 2024 spot weld cools to room temperature. A 9th power polynomial regression analysis was used to extrapolate the temperature output to that conforming with the stir zone temperature (490°C), see below.



The calculation method employed during the cooling period following spot welding is illustrated below:



The cooling curve obtained from the regression was divided into about 10°C increments and the diffusion rate (D_n) at each temperature (T_n) was obtained. The mass loss by particles in the stir zone during cooling was calculated from the diffused radius during each time increment, see the above figure.

During the first time interval (from t_{1s} to t_{1e}) the diffused radius is calculated using D_1 :

$$R_1 = R_0 \sqrt{1 - \frac{kD_1}{R_0^2} t_{1e}}$$

$$t_1 = t_{1e} - t_{1s}$$

In each successive time interval, the diffusion radius was obtained by taking account of the previous interval effect. For example, the second time interval (from t_{2s} to t_{2e}) was calculated using D_2 :

$$t_{2s} = \frac{R_0^2 - R_1^2}{kD_2}$$

$$R_2 = R_0 \sqrt{1 - \frac{kD_2}{R_0^2} t_{2e}}$$

$$t_2 = t_1 + (t_{2e} - t_{2s})$$

The radius after cooling (R_n) was calculated during the final n th time interval.

References

1. Thomas WM, Nicholas ED, Needham JD, Murch MG, Temple-smith P, Daws CJ (1991) G.B. Patent Application No. 9125978.8, Dec. 1991; U.S. Patent No. 5460317, Oct. 1995
2. Mishra RS, Ma ZY (2005) Mater Sci Eng R 50:1
3. Woo W, Choo H, Brown DW, Liaw P K, Feng Z (2006) Scripta Mater 54(11):1859
4. Ramirez AJ, Juhas MC (2003) Mater Sci Forum 426–432(Part 4):2999
5. Andersson CG, Andrews RE, Dance BGI, Russell MJ, Olden EJ, Sanderson RM (2000) In: Proceedings 2nd Int. Symp. on Friction Stir Welding, Gothenburg, Sweden, 2000
6. Cho J-H, Dawson PR (2006) Met Mater Trans A 37A(4):1147
7. Strand SR, Sorensen CD, Nelson TW (2003) In: Proceedings ANTEC 2003 Conference, 2003, p 1078
8. Cavaliere P (2006) J Mater Sci 41:4299
9. Lockwood WD, Tomaz B, Reynolds AP (2002) Mater Sci Eng A 323(1–2):348
10. Sutton MA, Yang B, Reynolds AP, Taylor R (2002) Mater Sci Eng A 323(1–2):160
11. Cederqvist L, Reynolds AP (2001) Weld J 80(12):281s
12. Reynolds AP, Tang W (2001) In: Proceedings Friction Stir Welding and Processing Symposium. Indianapolis, USA, 2001, p 15
13. Sato Y, Kokawa H (2001) Weld Int 15(9):693
14. Biallas G, Braun R, Dalle Donne C, Staniek G, Kaysser WA (1999) In: Proceedings of 1st Int. Symp. on Friction Stir Welding, Thousand Oaks, 1999

15. Zettler R, Lomolino S, Dos Santos JF, Donath Beckmann TF, Lippman T, Lohwasser D (2005) *Weld World* 49(3–4):41
16. Starink ML, Wang SC, Sinclair I (2005) *Friction Stir Welding and Processing III*. In: Jata KV et al TMS (2005) 233
17. Schilling C, Dos Santos J (2001) International Patent Publication No. WO 01/36144A1, May 25, 2001
18. Gerlich A, Su P, North TH (2005) *J Mater Sci* 40(24):6473
19. Sakano R, Murakami K, Yamashita K, Hoyoie T, Fujimoto M, Inuzuka M, Nagao Y, Kashiki H (2001) In: Proc. 7th Int. Symp. JWS, 2001, 645
20. Lin P-C, Lin S-H, Pan J, Pan T, Nicholson JM, Garman MA (2004) SAE Technical Series, 2004-01-1330
21. Su P, Gerlich A, North TH (2005) SAE Technical Series, 2005-01-1255
22. Frigaard Ø, Grong Ø, Hjelen J, Gulbrandsen-Dahl S, Midling OT (1999) In: Proc. 1st Internat. Symp. on Friction Stir Welding, Thousand Oaks, USA, 1999, TWI
23. TH North, GJ Bendzsak, CB Smith, GH Luan (2001) In: Proc. of the 7th Int. Symp. JWS, Kobe, Japan, 2001, 621
24. Hassan KhAA, Prangnell PB, Norman AF, Price DA, Williams SW (2003) *Sci Tech Weld Joining* 8:257
25. Gerlich A, Cingara GA, North TH (2006) *Met Trans A* 37A:2773
26. Schmidt H, Hattel J (2005) In: *Friction stir welding and processing III*, ed. (2005) 225
27. Su P, Gerlich A, North TH, Bendzsak GJ (2006) *Sci Tech Weld Joining* 11(2):163
28. Su P, Gerlich A, North TH, Bendzsak GJ (2006) SAE Technical Series, 2006-01-0971
29. Gerlich A, Cingara GA, North TH (2006) *Mater Sci Forum* 519–521:1107
30. Gerlich A, Su P, North TH, Bendzsak GJ (2006) In: Proc. Friction Stir Welding Colloquium, Graz, Austria, 23 May 2006
31. Jones MJ, Heurtier P, Desrayaud C, Montheillet F, Allehaux D, Driver JH (2005) *Scripta Mater* 52:693
32. Bowden FP, Ridler KEW (1936) *Proc R Soc Lond Ser A* 154(883):640
33. Bowden FP, Thomas PH (1954) *Proc R Soc Lond Ser A* 223(1152):29
34. Mcqueen HJ, Jonas JJ (1975) *Treatise on materials science technology*, vol 6. Academic Press, New York, N.Y., 393
35. Mcqueen HJ, Hockett JE (1970) *Metall Trans A* 1:2997
36. Avramovic-Cingara G, Mcqueen HJ, Hopkins A, Jain V, Perovic D Light weight alloys for aerospace applications. In: Lee EW et al (eds) TMS-AIME, 333
37. Avramovic-Cingara G, Mcqueen HJ (1994) *Aluminium* 70(3):214
38. Avramovic-Cingara G, Perovic DD, Mcqueen HJ (1996) *Metall Mater Trans* 27A:3478
39. Cerri E, Evangelista E, Forcellese A, Mcqueen HJ (1995) *Mater Sci Eng A* 197:181
40. Sheppard T (1990) In: Chen CQ, EA Starke EA (eds) Second Int. Conf. on Aluminum Alloys – Their Physical and Mechanical Properties. International Academic Publisher, p 744
41. Sheppard T (1987) In: Leoben-Wien (ed) Proc. 8th Light Metal Congress (8 Internationale Leichtmetalltagung), 1987, 301
42. Yang B, Yan J, Sutton M, Reynolds AP (2004) *Mater Sci Eng A* 364:55
43. ASM Metals Handbook, 8th edn (1961) 938
44. Benavides Y, Li Y, Murr LE, Brown D, Mcclure JC (1999) *Scripta Mater* 41(8):809
45. Charit I, Mishra RS (2003) *Mater Eng A* 359:290
46. Jones MJ, Heurtier P, Desrayaud C, Montheillet F, Allehaux D, Driver JH (2005) *Scripta Mater* 52:693
47. Karlsen M, Frigaard Ø, Hjelen J, Grong Ø, Norum H (2003) *Mater Sci Forum* 426–432:2861
48. Norman AF, Brough I, Prangnell PB (2000) *Mater Sci Forum* 331–337:1713
49. Sutton MA, Reynolds A P, Wang D-Q, Hubbard CR (2002) *J Eng Mater Technol* 124:215
50. Humphreys FJ, Hatherly M (1995) *Recrystallization and related annealing phenomena*. Pergamon Press, Oxford
51. Cohen M, Montheillet F (1979) Rapport ATP CNRS, contract No. 3136 (1979)
52. Kocks UF (1998) *Texture and anisotropy*. Cambridge University Press
53. Heurtier P, Desrayaud C, Montheillet F (2002) *Mater Sci Forum* 396–402:1537
54. North TH, Bendzsak GJ, Gerlich A, Su P, Maldonado C (2005) AWJT'2005 Conference, Dalian, PR China, 2005
55. North TH, Bendzsak GJ, Gerlich A, Su P, Cingara G (2006) THERMEC 2006. Vancouver, Canada, 2006
56. Pérez-Prado MT, González-Doncel G, Ruano OA, Mcnelley TR (2001) *Acta Mater* 49(12):2259
57. Fonda RW, Bingert JF, Colligan KJ (2004) *Scripta Mater* 51:243
58. Sato YS, Urata M, Kokawa H (2002) *Metall Mater Trans A* 33A:625
59. Droenen P-E, Ryum N (1994) *Met Trans A* 25A:521
60. Reiso O, Øverlie H-G, Ryum N (1990) *Met Trans A* 21A:1689
61. Li X-M, Starink MJ (2001) *Mater Sci Tech* 17:1324
62. Dalle-Donne C, Braun B, Staniek G, Jung A, Kayser WA (1998) *Materialwiss Werkst* 29:609
63. North TH, Bendzsak GJ, Smith CB (2000) In: Proc. 2nd Int. Conf. Friction Stir Welding, Gothenburg, Sweden, 2000, TWI
64. Gerlich A, Su P, North TH (2005) *Sci Tech Weld Joining* 10:647
65. Sato YS, Hwan S, Park C, Michiuchi M, Kokawa H (2004) *Scripta Mater* 50(9):1233
66. Cavaliere P, Cerri E, Squillace A (2005) *J Mater Sci* 40:3669
67. Whelan MJ (1969) *Met Sci J* 3:95
68. Brooks CR (1982) Heat treatment, structure and properties of nonferrous alloys, ASM Int128
69. Smithells CJ (1992) In: Brandes EA, Brook GB (eds) *Metals reference book: 7th edn*. Butterworth-Heinemann Ltd., p 13
70. Tundal U, Reiso O, Ryum N (1994) In: Fourth Int. Conf. on Aluminum Alloys (ICAA4), (1994) 590
71. Su J-Q, Nelson TW, Mishra M, Mahoney M (2003) *Acta Mater* 51:713
72. Su P, Gerlich A, North TH, Bendzsak GJ (2006) *Sci Tech Weld Joining* 11(1):61
73. Su P, Gerlich A, North TH, Bendzsak GJ (2007) *Met Trans A* (in press)